

# Timesaving phase retrieval approach based on difference map normalization and fast iterative algorithm

Yu Zhang<sup>a,b,\*</sup>, Xiaobo Tian<sup>c</sup>, Rongguang Liang<sup>c</sup>

<sup>a</sup> Institute of Materials Physics, College of Science, Northeast Electric Power University, Jilin, Jilin 132012, China

<sup>b</sup> State Key Laboratory of Applied Optics, Changchun Institute of Optics, Fine Mechanics and Physics, Chinese Academy of Sciences, Changchun, Jilin 130022, China

<sup>c</sup> College of Optical Sciences, University of Arizona, Tucson, Arizona 85721, USA

## ARTICLE INFO

### Keywords:

Phase shifting algorithm  
Iterative algorithm  
Difference map normalization  
Phase shift  
Interferometry

## ABSTRACT

To achieve high measurement accuracy with less computational time in phase shifting interferometry, a random phase retrieval approach based on difference map normalization and fast iterative algorithm (DN&FIA) is proposed, it doesn't need pre-filtering, and has the advantage of the iterative algorithms-high accuracy, moreover, it also has the advantage of non-iterative algorithms-timesaving, it only needs three randomly phase shifted interferograms, and the initial phase shifts of the iteration can be random, last but not least, it is effective for the circular, straight or complex fringes. The simulations and experiments verify the correctness and feasibility of DN&FIA.

## 1. Introduction

Since the optical phase distribution can be easily extracted by several interferograms, the phase shifting interferometry (PSI) has been widely used in optical measurement [1–3]. The accuracy of PSI mainly depends on the interferometer, environment and phase shifting algorithm (PSA), for the fixed interferometer and environment, the performance of PSA is very important to the accuracy of PSI, outstanding PSA can be applied to suppress the different kinds of errors, such as the miscalibration of piezo-transducer (PZT), detector error, vibrational error, air turbulence in the working environment, instability of the laser, and so on [4–6].

To date, the PSA can be divided into two types. The first type is the fixed-step PSA which can obtain the phase distribution by a series of phase shifted interferograms with equal and known phase shifts. This kind of algorithm needs at least three phase shifted interferograms, moreover, it can work well only when the phase shift is equal to the pre-set value, otherwise, a large error or deviation of phase retrieval will appear. Hence, this kind of algorithm is suitable for the situation with outstanding interferometer and stable environment. 3-step, 4-step, 5-step, and N-step PSAs etc. are all the outstanding fixed-step algorithms [4].

The second type is the random PSA. This kind of algorithm is suitable for the general interferometer and environment since it can overcome the phase shift error due to the miscalibration of PZT, vibrational error, air turbulence, instability of the laser frequency. For the random PSA, it can be divided into the iterative and non-iterative PSAs. Generally, the accuracy of the iterative PSA is relatively high, but it costs

more time because of the iterative operation. In 2004, an advanced iterative algorithm (AIA) based on a least-squares iterative procedure was introduced to extract phase distribution from randomly phase shifted interferograms [7]. It copes with the limitation of the existing iterative algorithms by separating a frame-to-frame iteration from a pixel-to-pixel iteration, and provides stable convergence and accurate phase extraction. In 2008, Xu et al. [8] presented an advance iterative algorithm to extract phase distribution from randomly and spatially non-uniform phase shifted interferograms, this algorithm divides the interferograms into small blocks and retrieves local phase shifts accurately by iterations. In 2013, an iterative PSA based on the least-squares principle was developed to overcome the random piston and tilt wavefront errors generated from the phase shifter [9]. In general, for optical metrology, especially for the in-situ metrology, the instantaneity of PSA is very important, while the iterative PSA costs more time, hence, only a small number of iterative PSAs have been developed.

The non-iterative PSA spends less time than the iterative PSA, but the accuracy may be not as high as the iterative PSA. In 1992, Farrell and Player [10] utilized Lissajous figures and ellipse fitting to calculate the phase difference between two interferograms, and in 2016, Liu et al. [11] proposed a PSA which can simultaneously extract the tested phase and phase shift from only two interferograms using Lissajous figure and ellipse fitting technology, but these two algorithms both need pre-filtering and the non-uniform intensity distribution will affect the accuracy. From 2003 to 2014, Cai et al. [12–20] proposed a series of statistical algorithms which can extract the phase shifts and tested phase, however, most of these algorithms need to know the

\* Corresponding author.

E-mail address: [521zhangyu2008@163.com](mailto:521zhangyu2008@163.com) (Y. Zhang).

intensities of object and reference. From 2011 to 2017, [21–27] proposed a series of PSAs based on principal component analysis (PCA) which is an efficient technique for phase extraction by converting a set of possibly correlated variables into a set of values of uncorrelated variables, but it cannot determine the global sign of the measured phase, and it needs more than three interferograms because it need to subtract relatively accurate mean. In 2012, [28] presented a two-step demodulation based on the Gram-Schmidt orthonormalization method (GS2), it requires subtracting the DC term by filtering before performing GS2. In 2014, Wang et al. [29] proposed an advanced GS method called GS3, the major advantage of this method is that it performs well when the phase shift is close to  $\pi$  as most two-step algorithms become invalid in this situation. Although non-iterative PSA costs less time than the iterative PSA, some non-iterative PSAs also spend more time on the pre-filtering or the determination of the global sign of the measured phase (PCA), hence, saving time is essential for both the iterative and non-iterative PSAs.

To achieve the high measurement accuracy with less time, the PSA is critical. For the non-iterative PSA with less than three phase shifted interferograms, it is difficult to obtain the high accuracy. For the iterative PSA, it can obtain the high accuracy, but it needs more time. To balance the computational time and accuracy, the research of iterative PSA with less time is essential.

In this paper, we will discuss the accurate and timesaving phase retrieval approach with unknown phase shifts. Section 2 presents the principle and process of the proposed PSA based on difference map normalization and fast iterative algorithm (DN&FIA). In Section 3 the simulation of DN&FIA is discussed, and the comparison with AIA is performed. Section 4 evaluates the novel PSA with the experimental data. The conclusion is finally drawn in Section 5.

## 2. Principles

### 2.1. Principle of the difference map normalization (DN)

In PSI, the intensity distribution of the phase shifted interferograms can be expressed as:

$$I_{ij} = a_{ij} + b_{ij} \cos(\varphi_j + \theta_i) \quad (1)$$

where  $i=1,2,\dots,P$  represents the image index with  $P$  the total number of phase shifted interferograms,  $P$  is set to 3, for simplicity, we use a single symbol  $j=1,2,\dots,Q$  to denote the bidimensional pixel position with  $Q$  the total number of pixels,  $a_{ij}$  and  $b_{ij}$  respectively represent the background intensity and modulation amplitude,  $\varphi_j$  is the tested phase, and  $\theta_i$  represents the phase shift between interferograms. Because there is only a piston  $\theta_1$  between  $\varphi_j$  and  $\varphi_j + \theta_1$ , which doesn't affect the phase distribution, for simplicity, we define  $\theta_1 = 0$  in the following discussion.

Firstly, we implement the subtraction between the three phase shifted interferograms to filter the background intensity since the subtraction can cost less time than the filtering algorithm. Generally for the background intensity and modulation amplitude distributions, both the fluctuation between different interferograms and the non-uniformity between different pixels exist due to the instability of the light source, however, the subtraction can still filter most of the background intensity, hence, for simplicity, we assume that  $a_{ij}$  and  $b_{ij}$  are irrelevant to  $i$ , only relevant to  $j$  in the filtering process, so  $a_{1j} = a_{2j} = \dots = a_{Pj} = a_j$ ,  $b_{1j} = b_{2j} = \dots = b_{Pj} = b_j$ , and a best condition of this assumption can be given that it is best to use the light source with high stability or apply to the synchronous phase-shifting interferometer (SPSI).

Two difference maps between the 1st, 2nd, and 3rd interferograms can be defined as:

$$\begin{aligned} D_{1j} &= I_{1j} - I_{2j} = 2b_j \sin\left(\frac{\theta_2}{2}\right) \sin\left(\varphi_j + \frac{\theta_2}{2}\right) \\ &= 2b_j \sin\left(\frac{\theta_2}{2}\right) \cos\left(\Phi_j - \frac{\pi}{2}\right) = 2b_j \sin\left(\frac{\theta_2}{2}\right) \cos(\Phi'_j) \end{aligned} \quad (2)$$

$$\begin{aligned} D_{2j} &= I_{1j} - I_{3j} = 2b_j \sin\left(\frac{\theta_3}{2}\right) \sin\left(\varphi_j + \frac{\theta_3}{2}\right) \\ &= 2b_j \sin\left(\frac{\theta_3}{2}\right) \cos\left(\Phi_j + \Delta - \frac{\pi}{2}\right) = 2b_j \sin\left(\frac{\theta_3}{2}\right) \cos(\Phi'_j + \Delta) \end{aligned} \quad (3)$$

where  $\Phi_j = \varphi_j + \frac{\theta_2}{2}$ ,  $\Delta = \frac{\theta_3 - \theta_2}{2}$ ,  $\Phi'_j = \Phi_j - \frac{\pi}{2}$ .

Since the phase shifts between the different interferograms are different,  $\theta_2 \neq \theta_3$  and  $2b_k \sin(\frac{\theta_2}{2}) \neq 2b_k \sin(\frac{\theta_3}{2})$ , the amplitude of  $D_{1j}$  is different from  $D_{2j}$ . Hence, to eliminate the effect of the different amplitudes, the normalization is introduced to cope with two difference maps. Moreover, whether the Euclidean 2-norm or infinity norm can normalize the difference vectors  $D_{1j}$  and  $D_{2j}$ , we will choose the Euclidean 2-norm since we want to obtain the new phase shifted interference signals without the background intensity in the following.

Generally, the normalization of the vector  $u$  can be expressed as

$$\bar{u} = u / \sqrt{\langle u, u \rangle} = u / \|u\| \quad (4)$$

where  $\bar{u}$  represents the normalized vector,  $\|\cdot\|$  and  $\langle \cdot, \cdot \rangle$  respectively represent the 2-norm and the inner product.

Normalizing the two difference vectors  $D_{1j}$  and  $D_{2j}$ , we can obtain

$$\bar{D}_{1j} = \frac{D_{1j}}{\|D_{1j}\|} = \frac{b_j \cos(\Phi'_j)}{\sqrt{\sum_{j=1}^Q b_j^2 \cos^2(\Phi'_j)}} \quad (5)$$

$$\bar{D}_{2j} = \frac{D_{2j}}{\|D_{2j}\|} = \frac{b_j \cos(\Phi'_j + \Delta)}{\sqrt{\sum_{j=1}^Q b_j^2 \cos^2(\Phi'_j + \Delta)}} \quad (6)$$

If we have more than one fringe in the interferograms, we have the following approximation

$$\begin{aligned} &\sum_{j=1}^Q b_j^2 \cos^2(\Phi'_j) - \sum_{j=1}^Q b_j^2 \cos^2(\Phi'_j + \Delta) \\ &= \sum_{j=1}^Q b_j^2 \cdot [\cos(\Phi'_j) - \cos(\Phi'_j + \Delta)] \cdot [\cos(\Phi'_j) + \cos(\Phi'_j + \Delta)] \\ &= -4 \sum_{j=1}^Q b_j^2 \cdot \sin\left(\frac{2\Phi'_j + \Delta}{2}\right) \cdot \sin\left(\frac{-\Delta}{2}\right) \cdot \cos\left(\frac{2\Phi'_j + \Delta}{2}\right) \cdot \cos\left(\frac{-\Delta}{2}\right) \\ &= \sum_{j=1}^Q b_j^2 \cdot \sin(2\Phi'_j + \Delta) \cdot \sin(\Delta) \\ &\approx 0 \end{aligned} \quad (7)$$

Then we will have the approximation

$$\sqrt{\sum_{j=1}^Q b_j^2 \cos^2(\Phi'_j)} \approx \sqrt{\sum_{j=1}^Q b_j^2 \cos^2(\Phi'_j + \Delta)} \quad (8)$$

Then the above normalized difference vectors can be rewritten as

$$\bar{D}_{1j} = c_j \cos(\Phi'_j) \quad (9)$$

$$\bar{D}_{2j} = c_j \cos(\Phi'_j + \Delta) \quad (10)$$

$$\text{where } c_j = \frac{b_j}{\sqrt{\sum_{j=1}^Q b_j^2 \cos^2(\Phi'_j)}} = \frac{b_j}{\sqrt{\sum_{j=1}^Q b_j^2 \cos^2(\Phi'_j + \Delta)}}$$

$\theta_2$  cannot be equal to  $\theta_3$  since the phase shift must exist between different phase shifted interferograms, hence,  $\Delta$  is non-zero value, from Eqs. (9) and (10), we can see that  $\bar{D}_{1j}$  and  $\bar{D}_{2j}$  are just as two phase shifted interference signals without the background intensity,  $\Delta$  represents the phase shift between two new phase shifted interference signals, and  $c_j$  denotes the new modulation amplitude. Because of the fluctuation, non-uniformity of the original modulation amplitude  $b_{ij}$  and the approximation error of Eq. (8), the new modulation amplitude  $c_j$  are both relevant to the pixel positions and image index, hence Eqs. (8) and (9) are rewritten as

$$\bar{D}_{mj} = c_{mj} \cos(\Phi'_j + \Delta_m) \quad (11)$$

where  $m=1,2$  denotes the index of the new phase shifted interference signals,  $\Delta_1 = 0$  and  $\Delta_2 = \Delta$ .

We know that there is only a piston between  $\varphi_j$  and  $\Phi'_j$ , which doesn't affect the phase distribution, hence we can use  $\Phi'_j$  to express the tested phase.

### 2.2. Principle of the fast iterative algorithm(FIA)

After the difference map normalization (DN), we design a fast iterative algorithm (FIA) which can accurately extract the tested phase distribution with less computational time. In the following, we will introduce the proposed method in detail:

Step1: We select a limited number of samples at regular intervals from Eq. (11), the phase shifted signal with the chosen samples can be expressed as

$$\bar{D}'_{mn} = c_{mn} \cos(\Phi'_n + \Delta_m) \quad (12)$$

where  $n=1,2,\dots,N$  denotes the chosen pixel number with  $N$  the total number of chosen pixels.

Step 2: Provided that  $c_{mn}$  is irrelevant to  $m$ , only relevant to  $n$ , then  $c_{1,n} = c_{2,n} = c_n$ . By setting  $\eta_n = c_n \cos \Phi'_n$ , and  $\xi_n = -c_n \sin \Phi'_n$ , Eq. (11) can be rewritten as

$$\bar{D}'_{mn} = \eta_n \cos \Delta_m + \xi_n \sin \Delta_m \quad (13)$$

The sum of squared differences between the theoretical and actual value of the phase shifted signal can be expressed as

$$S_n = \sum_{m=1}^2 (\bar{D}'_{mn} - \bar{D}_{mn})^2 = \sum_{m=1}^2 (\eta_n \cos \Delta_m + \xi_n \sin \Delta_m - \bar{D}_{mn})^2 \quad (14)$$

where  $\bar{D}_{mn}$  is actual value of the difference phase shifted signal obtained by the experimental data.

According to the least-squares theory [7–9],  $S_n$  should be minimum, for the known  $\Delta_1$  and  $\Delta_2$ ,  $\partial S_n / \partial \eta_n = 0$ ,  $\partial S_n / \partial \xi_n = 0$ , so

$$X_n = T^{-1} R_n \quad (15)$$

$$T = \begin{bmatrix} \sum_{m=1}^2 \cos^2 \Delta_m & \sum_{m=1}^2 \sin \Delta_m \cos \Delta_m \\ \sum_{m=1}^2 \sin \Delta_m \cos \Delta_m & \sum_{m=1}^2 \sin^2 \Delta_m \end{bmatrix} \quad (16)$$

$$X_n = [\eta_n \quad \xi_n]^T \quad (17)$$

$$R_n = \left[ \sum_{m=1}^2 \bar{D}_{mn} \cos \Delta_m \quad \sum_{m=1}^2 \bar{D}_{mn} \sin \Delta_m \right]^T \quad (18)$$

$\eta_n$  and  $\xi_n$  can be obtained by Eq. (15), and the tested phase can be calculated by

$$\Phi'_n = \tan^{-1} \left( -\frac{\xi_n}{\eta_n} \right) \quad (19)$$

To further save time, the unwrapped process is ignored, and we only need to justify the quadrant of the phase  $\Phi'_n$ .

Step 3: Provided that  $c_{mn}$  is irrelevant to  $n$ , only relevant to  $m$ , so  $c_{m1} = c_{m2} = \dots = c_{mN} = c_m$ . By setting  $\eta_m = c_m \cos \Delta_m$ , and  $\xi_m = -c_m \sin \Delta_m$ , Eq. (12) becomes

$$\bar{D}'_{mn} = \eta_m \cos \Phi'_n + \xi_m \sin \Phi'_n \quad (20)$$

The squared sum of the differences between the theoretical and actual value of the difference phase shifted signal can be expressed as

$$S_m = \sum_{n=1}^N (\bar{D}'_{mn} - \bar{D}_{mn})^2 = \sum_{n=1}^N (\eta_m \cos \Phi'_n + \xi_m \sin \Phi'_n - \bar{D}_{mn})^2 \quad (21)$$

For the known  $\Phi'_n$ , the least-squares criterion yields

$$X_m = T'^{-1} R_m \quad (22)$$

$$T' = \begin{bmatrix} \sum_{n=1}^N \cos^2 \Phi'_n & \sum_{n=1}^N \sin \Phi'_n \cos \Phi'_n \\ \sum_{n=1}^N \sin \Phi'_n \cos \Phi'_n & \sum_{n=1}^N \sin^2 \Phi'_n \end{bmatrix} \quad (23)$$

$$X_m = [\eta_m \quad \xi_m]^T \quad (24)$$

$$R_m = \left[ \sum_{n=1}^N \bar{D}_{mn} \cos \Phi'_n \quad \sum_{n=1}^N \bar{D}_{mn} \sin \Phi'_n \right]^T \quad (25)$$

$\eta_m$  and  $\xi_m$  can be obtained by Eq. (22), and the phase shift of two new phase shifted interference signals can be calculated by

$$\Delta_m = \tan^{-1} \left( -\frac{\xi_m}{\eta_m} \right) \quad (26)$$

Step 4: Repeat steps 2 and 3 until  $|\Delta_m^k - \Delta_m^{k-1}| - |\Delta_m^{k-1} - \Delta_m^{k-2}| < \varepsilon$ , the iteration terminates, and the accurate phase shifts can be obtained, where  $\varepsilon$  is the predefined converging threshold of iteration, i.e.,  $10^{-5}$  rad, and  $k$  represents the number of iterations.

Step 5: Perform step 2 using the extracted phase shifts and the whole samples of Eq. (11), then the accurate phase distribution can be obtained, note that, the unwrapped process is needed in the final step, and this is the only unwrapped process in the proposed method.

Note that, the new parameter  $c_{mn}$  is relevant to both  $m$  and  $n$ , for one pixel, there are five unknowns which are  $c_{1n}$ ,  $c_{2n}$ ,  $\Delta_1$ ,  $\Delta_2$  and  $\Phi'_j$ , but we have only two equations, we can't calculate the phase distribution, hence, we assume that  $\Delta_1$ ,  $\Delta_2$  are known and the new parameter  $c_{mn}$  is irrelevant to  $m$ , only relevant to  $n$  to calculate the tested phase, then we assume that  $c_{mn}$  is irrelevant to  $n$ , only relevant to  $m$  to calculate the phase shift, then use the iterations to decrease the error of the assumptions, and obtain the relatively accurate result.

The proposed method is an iterative algorithm, but it costs less time, there are three reasons, firstly, the background intensity is filtered by implementing the subtraction between the three phase shifted interferograms, this process costs less time than the filtering algorithm, moreover, FIA doesn't need to calculate the background intensity to further save time, secondly, only a limited number of samples are chosen to take part in the iterative process, this method saves most of time, lastly, only one time of unwrapped process is used in the whole calculation, this timesaving method is often used in the iterative algorithm. Moreover, the first two reasons are also the differences between the proposed method and AIA.

### 3. Simulation

To verify the effectiveness of the method proposed above, we perform a series of numerical simulations, and compare it with the well-evaluated method AIA. In the following, all computations are performed with the CPU of Intel(R) Core(TM) i7-6700 and the 8 GB memory, and we use the Matlab software for coding.

Firstly, we test the method with different kinds of fringes, including circular, straight and complex fringes. The background intensity and modulation amplitude are set as  $a_i(x, y) = N_a \exp[-0.02(x^2 + y^2)]$  and  $b_i(x, y) = N_b \exp[-0.02(x^2 + y^2)]$  respectively, where  $-1 \leq x \leq 1, -1 \leq y \leq 1$ . Generally, the background intensity and modulation amplitude have frame-to-frame fluctuation, hence,  $N_a$  of the 1st, 2nd and 3rd interferograms are set as 1, 0.95 and 0.9,  $N_b$  of the 1st, 2nd and 3rd interferograms are set as 0.9, 0.85 and 0.8. For the circular fringes, the tested phase is set as  $\varphi = N_f \pi(x^2 + y^2)$ , in which  $N_f = 5$  is the fringe number in the interferogram. The phase shifts of the three phase shifted interferograms are preset as 0 rad, 1.5 rad and 3.5 rad respectively. Moreover,

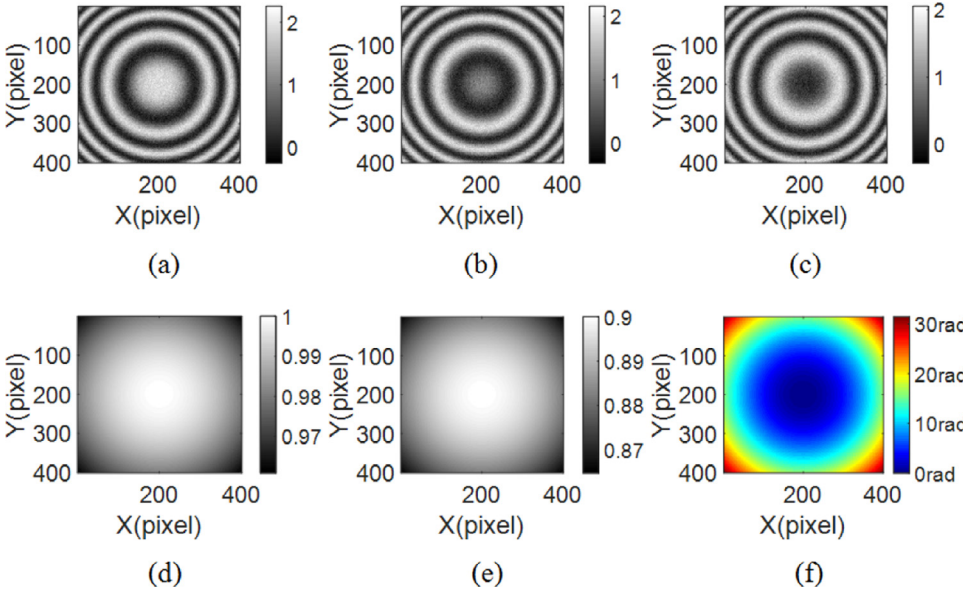


**Fig. 1.** Simulated interferograms with the circular fringes, background intensity, modulation amplitude and reference phase distribution. (a), (b) and (c) the three phase shifted interferograms, (d) and (e) the simulated background intensity and modulation amplitude of the first phase shifted interferogram, (f) the reference phase distribution (PV = 31.416 rad, RMS = 6.656 rad).

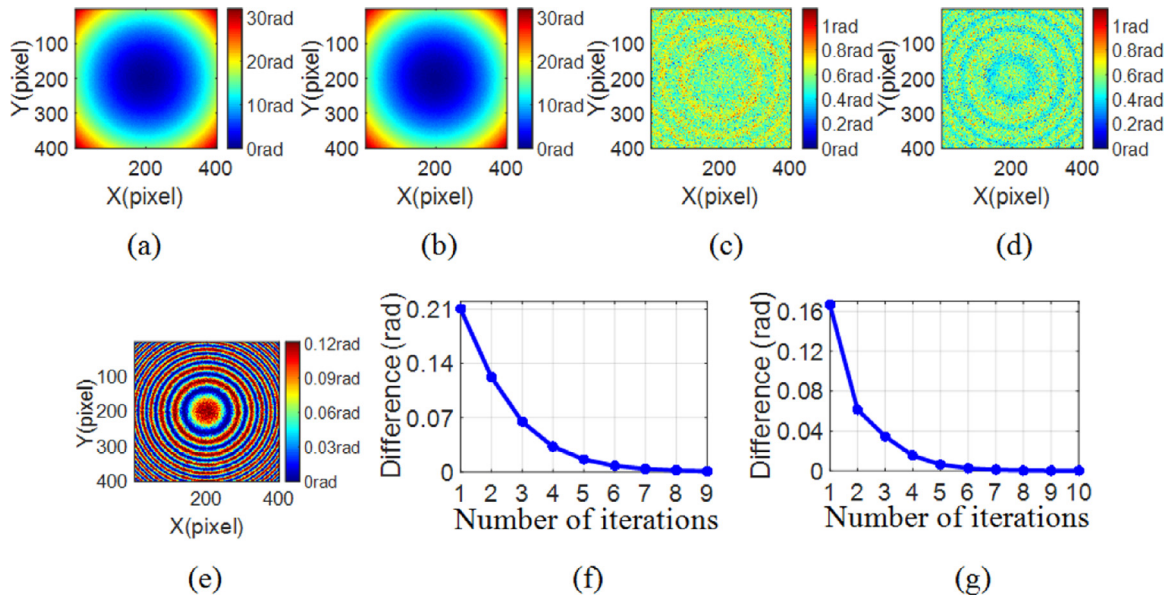


**Fig. 2.** Simulated results of the circular fringes. (a) and (b) the phase distributions extracted by DN&FIA (PV = 31.929 rad, RMS = 6.663 rad) and AIA (PV = 31.927 rad, RMS = 6.663 rad), (c) and (d) the phase error distributions after using DN&FIA and AIA, (e) the difference between the extracted phase distributions by DN&FIA and AIA, (f) and (g) the iterative curves of DN&FIA and AIA.

the Gaussian noise with a signal-to-noise ratio (SNR) of 20 dB generated by the function *awgn* in Matlab is added to the interferograms. With the above parameters setting, three simulated phase shifted interferograms with the size of  $401 \times 401$  are generated, as shown in Figs. 1(a)–(c), and the background intensity and modulation amplitude distributions of the first phase shifted interferogram are shown in Figs. 1(d) and (e), the reference phase distribution is illustrated in Fig. 1(f).

Then we respectively use DN&FIA and AIA to extract the tested phase distribution. For DN&FIA, the initial phase shifts of the iteration are respectively set as 0 rad and 0.5 rad, and only  $41 \times 41$  pixels are uniformly selected to take part in the iterative process, it will highly save time. And, the initial phase shifts of the iteration for AIA are respectively set as 0 rad, 1 rad and 3 rad. In addition, the predefined converging threshold of iteration for DN&FIA and AIA is  $10^{-5}$  rad. Fig. 2(a) and (b) show the phase distributions extracted by DN&FIA and AIA, and the phase error distributions are shown in Fig. 2(c) and (d). The RMS phase er-

rors of DN&FIA (0.1179 rad) and AIA (0.1231 rad) are similar, and the difference between the phase distributions extracted by two methods is shown in Fig. 2(e), the RMS value is only 0.0427 rad, that is to say, the accuracies of these two methods are similar. The iterative curves of DN&FIA and AIA are plotted in Figs. 2(f) and (g).

For the straight fringes, the theoretical phase is set as  $\varphi = N_s \pi x$ , in which  $N_s = 5$ , and for the complex fringes, the phase is set as  $\varphi = N_x \pi x + N_y \pi y + N_c \text{peaks}(401)$ , in which  $N_x = N_y = N_c = 5$ , other parameters are same as the circular fringes. Fig. 3 shows one of the simulated interferograms with the straight fringes and reference phase distribution. Fig. 4 represents the simulated results of the straight fringes using DN&FIA and AIA. For the complex fringes which are asymmetrical, as shown in Fig. 5(a), the complex phase distribution is drawn in Fig. 5(b), and the simulated results are shown in Fig. 6. For the straight fringes, the RMS phase errors of DN&FIA and AIA are 0.1179 rad and 0.1235 rad, and the RMS value of the difference between the phase

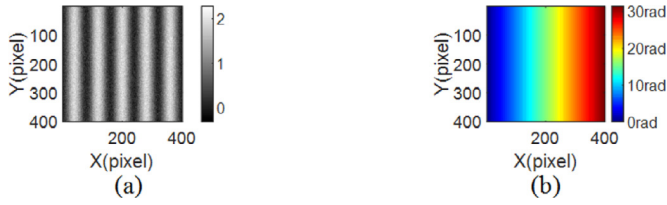


Fig. 3. Simulated interferogram with the straight fringes and reference phase distribution. (a) One of the simulated interferograms, (b) reference phase distribution (PV = 31.416 rad, RMS = 9.092 rad).

distributions extracted by two methods is 0.0347 rad. For the complex fringes, the RMS phase errors of DN&FIA and AIA are 0.1182 rad and 0.1232 rad, and the RMS value of the difference is 0.0319 rad. From the above simulations, we can get the conclusion as the circular fringes, the accuracies of two methods are similar.

Moreover, we compare the computational time for DN&FIA and AIA, the results are shown in Table 1. We can see that, the computational time of DN&FIA is further less than that of AIA. Hence, we get the conclusions that, DN&FIA is suitable for the circular, straight and complex fringes, and it can obtain relatively accurate phase distribution as AIA with less time.

Secondly, we perform the proposed method with different chosen samples to compare the accuracy and computational time, the computational time and RMS phase errors of the circular, straight and complex fringes with different chosen samples are shown in Table 2, where T and P represent computational time and RMS phase error, and Cir, Str and Com represent the circular, straight and complex fringes. For the different fringes with the same number of chosen samples, the computational time is similar because the processing time only depends on the number of chosen pixels, and the computational time is increasing with the increase of chosen samples, however, the RMS phase errors are stable when the chosen pixels are more than  $41 \times 41$ , hence, for the samples with  $401 \times 401$ , the best chosen samples are  $41 \times 41$ , it can obtain high accuracy and cost less computational time simultaneously. Moreover, for different fringes, when the chosen samples are less than  $41 \times 41$ , there are some differences, the results of the circular fringes are relatively stable for different chosen pixels, but for the straight and com-



Fig. 5. Simulated interferogram with the complex fringes and reference phase distribution. (a) One of the simulated interferograms, (b) reference phase distribution (PV = 89.375 rad, RMS = 18.359 rad).

plex fringes, when the chosen samples are too few, the phase errors are relatively large since the fringes are asymmetric, that is to say, when the chosen samples are less than  $41 \times 41$ , for the straight and complex fringes, different chosen samples will affect the accuracy, but for the symmetric circular fringes, different chosen samples will slightly affect the accuracy.

Thirdly, provided that the tested phase distribution  $\varphi = N_f \pi(x^2 + y^2)$ , which  $N_f$  represents the fringe number in one interferogram. In Section 2, in order to meet the approximation in Eq. (8), we assume that there is more than one fringe in the interferogram, in the following, we vary the fringe numbers while fixing the SNR to 20 dB to obtain the best range of the fringe numbers using DN&FIA. As can be seen from Table 3, when the fringe number is less than 0.7, the RMS phase error is relatively larger, and the ratio of RMS phase to RMS phase error is also larger. For the range of fringe numbers between 0.8 and 2.0, the RMS phase error is unstable. When the fringe numbers are more than 2, the RMS phase errors are similar, in this case, the approximation error is nearly stable, hence, we can conclude that the fringe numbers are best to be more than 2 if high accuracy is requested.

Then, we study the proposed method with the different initial phase shifts, the conditions are same as the above circular fringes. According to the Eqs. (9) and (10), we know that the relative phase shift between two new interference signals is  $\frac{\theta_3 - \theta_2}{2}$ , so the theoretical value of the relative phase shift for the proposed method is 1 rad. The number of iterations and computational time of different initial phase shifts are plotted in Fig. 7. Through the simulation, we found that the RMS phase errors are same for the different initial phase shifts, they are 0.1179 rad. From Fig. 7, we can see that, the closer the initial phase shift is to the

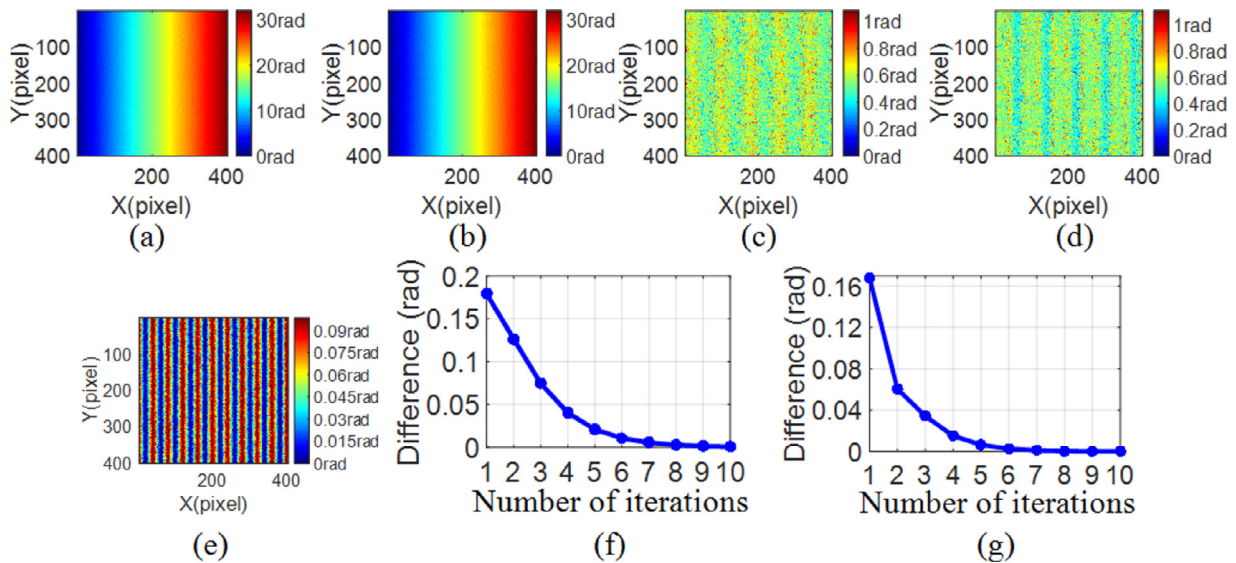
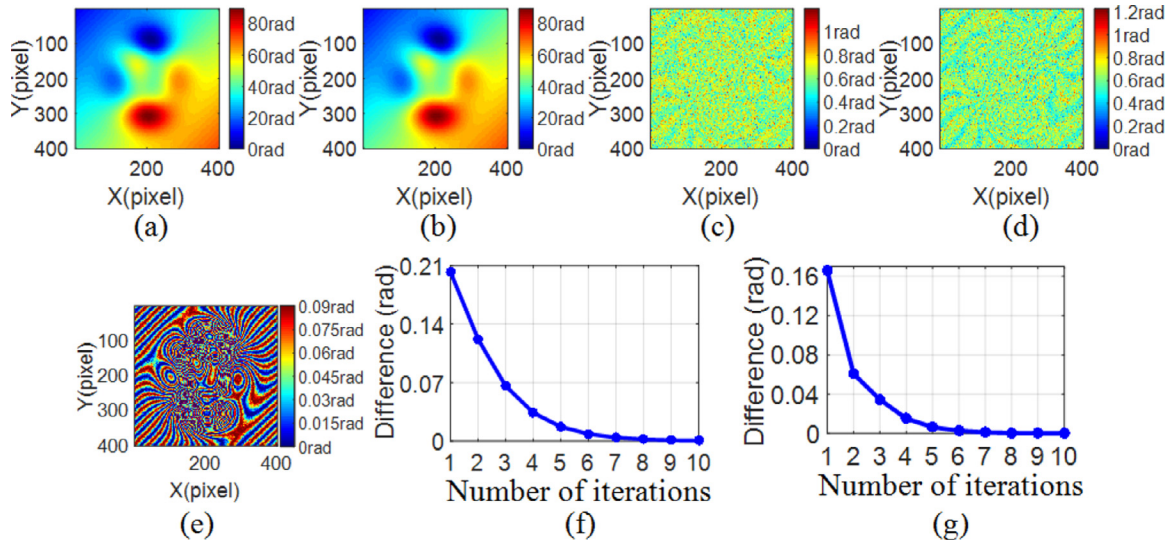


Fig. 4. Simulated results of the straight fringes. (a) and (b) the phase distributions extracted by DN&FIA (PV = 32.108 rad, RMS = 9.086 rad) and AIA (PV = 32.092 rad, RMS = 9.087 rad), (c) and (d) the phase error distributions after using DN&FIA and AIA, (e) the difference between the extracted phase distributions by DN&FIA and AIA, (f) and (g) the iterative curves of DN&FIA and AIA.



**Fig. 6.** Simulated results of the complex fringes. (a) and (b) the phase distributions extracted by DN&FIA (PV=89.732 rad, RMS=18.360 rad) and AIA (PV=89.716 rad, RMS=18.360 rad), (c) and (d) the phase error distributions after using DN&FIA and AIA, (e) the difference between the extracted phase distributions by DN&FIA and AIA, (f) and (g) the iterative curves of DN&FIA and AIA.

**Table 1**  
Computational time of different methods with different fringes.

| Time (s) | Circular fringes | Straight fringes | Complex fringes |
|----------|------------------|------------------|-----------------|
| DN&FIA   | 1.20             | 1.20             | 1.21            |
| AIA      | 17.09            | 17.28            | 17.00           |

theoretical phase shift, the less the number of iterations is, and the computational time is also least, however, the difference between the longest time and shortest time is only 0.07 s, it will hardly affect the efficiency of the proposed method, in addition, when the initial phase shift is equal to the theoretical phase shift, 6 iterations are also needed since the fluctuation between different interferograms and the non-uniformity between different pixels exist, and large noise is added to the interferograms. For most iterative algorithms, the initial value of iteration will affect the effectiveness of the algorithm, but DN&FIA can remove this restriction because different initial values will not affect the accuracy and the computational time will be only less affected, hence, the initial phase shifts of the iteration for DN&FIA can be set randomly.

We know that the phase shifts are important to the PSAs, hence, it is necessary to discuss the phase error due to different phase shifts for the proposed method. In order to get the general conclusion, we study the phase error due to different phase shifts with different situations and fringes. The phase shifts of the 1st and 2nd frames are respectively set as 0 rad and 1 rad while the phase shift of the 3rd frame is uniformly changed from 2.0 rad to 5.21 rad (the range of relative phase shift between the 2nd and 3rd interferograms is from 1 rad to 4.21 rad). In situation 1, only 20 dB noise is added to the phase shifted interferograms, and for the situation 2, except for the 20 dB noise, the background intensity and modulation amplitude are non-uniform,  $N_a$

and  $N_b$  of the three interferograms are set as 1 and 0.9. In situation 3, except for the 20 dB noise, for the background intensity and modulation amplitude, only the fluctuation between different interferograms exists,  $a_1 = 1, a_2 = 0.95, a_3 = 0.9, b_1 = 0.9, b_2 = 0.85, b_3 = 0.8$ . In situation 4, except for the 20 dB noise, both the fluctuation and non-uniformity of the background intensity and modulation amplitude exist,  $N_a$  of the 1st, 2nd and 3rd interferograms are set as 1, 0.95 and 0.9,  $N_b$  of the 1st, 2nd and 3rd interferograms are set as 0.9, 0.85 and 0.8. The simulated results are plotted in Fig. 8. From Fig. 8, we can come to the following conclusions: (1) for all the fringes, the RMS phase error in situation 4 is largest because situation 4 is most complex, the mixed errors cause the largest phase error, and situation 1 has the smallest error since it is simplest, moreover, the phase error in situation 3 is larger than that in situation 2, that is to say, the effect of the fluctuation between different interferograms is larger than that of the non-uniformity between different pixels for DN&FIA; (2) the RMS phase errors are different due to different phase shifts, while the phase shift is close to 2.0 rad, the RMS phase error is significantly large since small practical phase shift  $(\theta_3 - \theta_2)/2$  will introduce large phase error; (3) the corresponding phase shifts of the minimum RMS phase errors for different fringes and situations are same, it is 3.606 rad, the relative phase shift between 2nd and 3rd interferograms is 2.606 rad; (4) the curves of RMS phase errors are relatively smooth when the range of phase shift between the 1st and 3rd interferograms is from 2.64 rad to 4.57 rad, hence the above range of phase shift can be considered when the relatively high accuracy is demanded.

To study whether the correspondingly relative phase shift between the 2nd and 3rd interferograms of the minimum RMS phase errors is a constant, the phase shifts of the 1st and 2nd frames are respectively reset as 0 rad and 1.5 rad while the phase shift of the 3rd frame is uniformly changed from 2.5 rad to 5.71 rad, the range of relative phase shift be-

**Table 2**  
Computational time and RMS phase errors of different fringes with different chosen samples.

| Samples   | 6 × 6  | 11 × 11 | 21 × 21 | 41 × 41 | 81 × 81 | 101 × 101 | 201 × 201 | 401 × 401 |
|-----------|--------|---------|---------|---------|---------|-----------|-----------|-----------|
| Cir T (s) | 1.10   | 1.12    | 1.16    | 1.20    | 1.57    | 1.82      | 3.97      | 13.38     |
| P (rad)   | 0.1179 | 0.1181  | 0.1182  | 0.1179  | 0.1179  | 0.1179    | 0.1179    | 0.1179    |
| Str T (s) | 1.11   | 1.12    | 1.15    | 1.20    | 1.57    | 1.83      | 3.97      | 13.20     |
| P (rad)   | 0.1414 | 0.1563  | 0.1181  | 0.1179  | 0.1179  | 0.1179    | 0.1179    | 0.1179    |
| ComT (s)  | 1.12   | 1.13    | 1.17    | 1.21    | 1.59    | 1.85      | 4.00      | 13.05     |
| P (rad)   | 0.1187 | 0.1205  | 0.1184  | 0.1182  | 0.1182  | 0.1182    | 0.1182    | 0.1182    |

**Table 3**  
RMS phase and RMS phase errors with different fringe numbers using DN&FIA.

| Fringe numbers        | 0.5    | 0.6    | 0.7    | 0.8     | 0.9     | 1.0     | 1.1     | 1.2    |
|-----------------------|--------|--------|--------|---------|---------|---------|---------|--------|
| RMS phase (rad)       | 0.7822 | 0.8710 | 0.9728 | 1.0980  | 1.2323  | 1.3673  | 1.4643  | 1.5975 |
| RMS phase error (rad) | 0.1693 | 0.1472 | 0.1251 | 0.1176  | 0.1170  | 0.1176  | 0.1183  | 0.1195 |
| Fringe numbers        | 1.3    | 1.4    | 1.5    | 1.6     | 1.7     | 1.8     | 1.9     | 2.0    |
| RMS phase (rad)       | 1.7306 | 1.8637 | 1.9968 | 2.1300  | 2.2631  | 2.3962  | 2.5293  | 2.6625 |
| RMS phase error (rad) | 0.1219 | 0.1237 | 0.1237 | 0.1222  | 0.1199  | 0.1179  | 0.1184  | 0.1177 |
| Fringe numbers        | 3.0    | 4.0    | 5.0    | 15      | 25      | 35      | 45      |        |
| RMS phase (rad)       | 3.9937 | 5.3249 | 6.6561 | 19.9684 | 33.2807 | 46.5929 | 59.9052 |        |
| RMS phase error (rad) | 0.1175 | 0.1179 | 0.1179 | 0.1176  | 0.1175  | 0.1175  | 0.1177  |        |

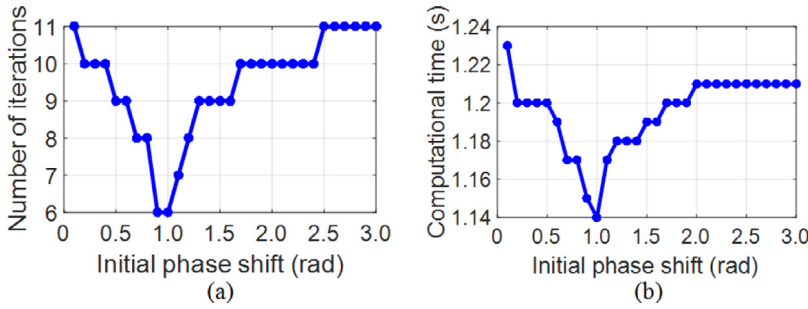


**Fig. 7.** The results of different initial phase shifts. (a) and (b) the number of iterations and computational time of different initial phase shifts.

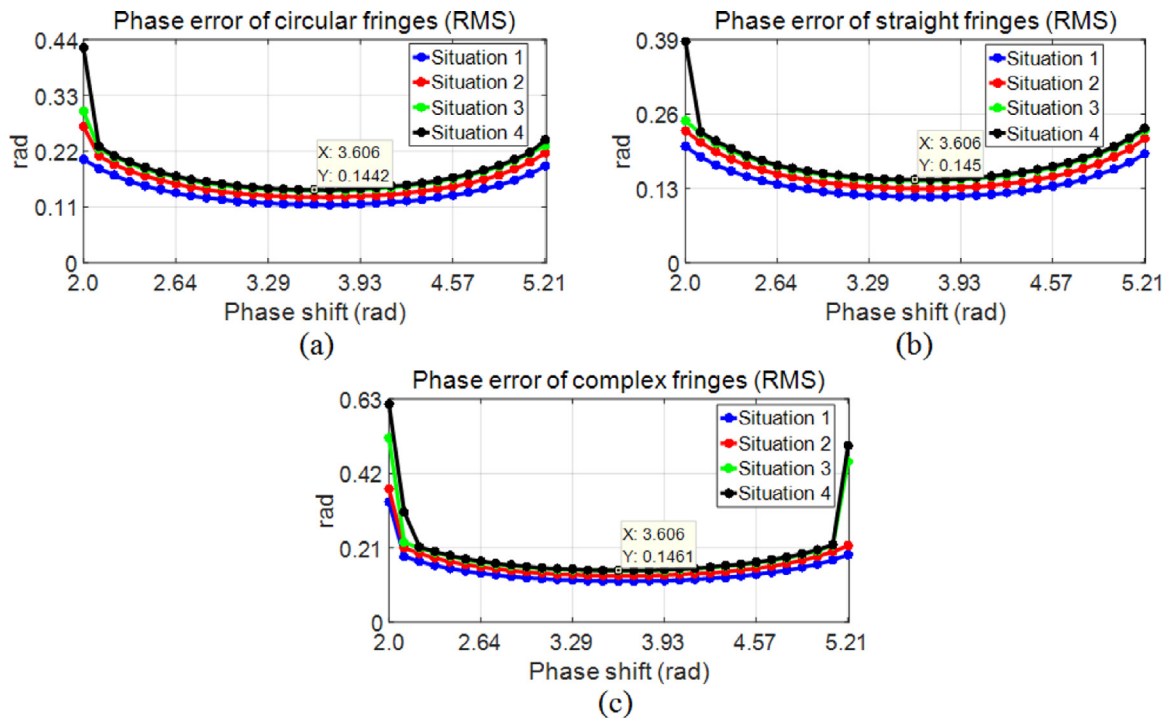


**Fig. 8.** The RMS phase errors of different phase shifts using DN&FIA ( $\theta_1 = 0, \theta_2 = 1$ ). (a), (b) and (c) RMS phase errors of the circular, straight and complex fringes with different phase shifts and situations.

tween the 2nd and 3rd interferograms is same as the above simulations, the results of the circular fringes are shown in Fig. 9(a), we can see that, the curves are similar to the above simulations, but the best phase shift of the 3rd interferogram is 3.892 rad, that is to say, the relative phase shift between the 2nd and 3rd interferograms is 2.392 rad, which is not equal to the above simulations, hence, the best relative phase shift between 2nd and 3rd interferograms is a variable value due to different relative phase shifts between 1st and 2nd interferograms, the best phase shift between 2nd and 3rd interferograms with the different phase shifts

between 1st and 2nd interferograms is plotted in Fig. 9(b), and for situation 4, the minimum RMS phase errors which are corresponding to the best phase shifts between 2nd and 3rd interferograms is plotted in Fig. 9(c). From Fig. 9(b) and (c), we can see that, for the simulated conditions, when the phase shift between 1st and 2nd interferograms is 2 rad, and the phase shift between 2nd and 3rd interferograms is 2.071 rad, the RMS phase error is minimum, it is 0.1095 rad.

In addition, the relationship between the best phase shift and fringe numbers is studied, we simulate the circular fringes when the fringe

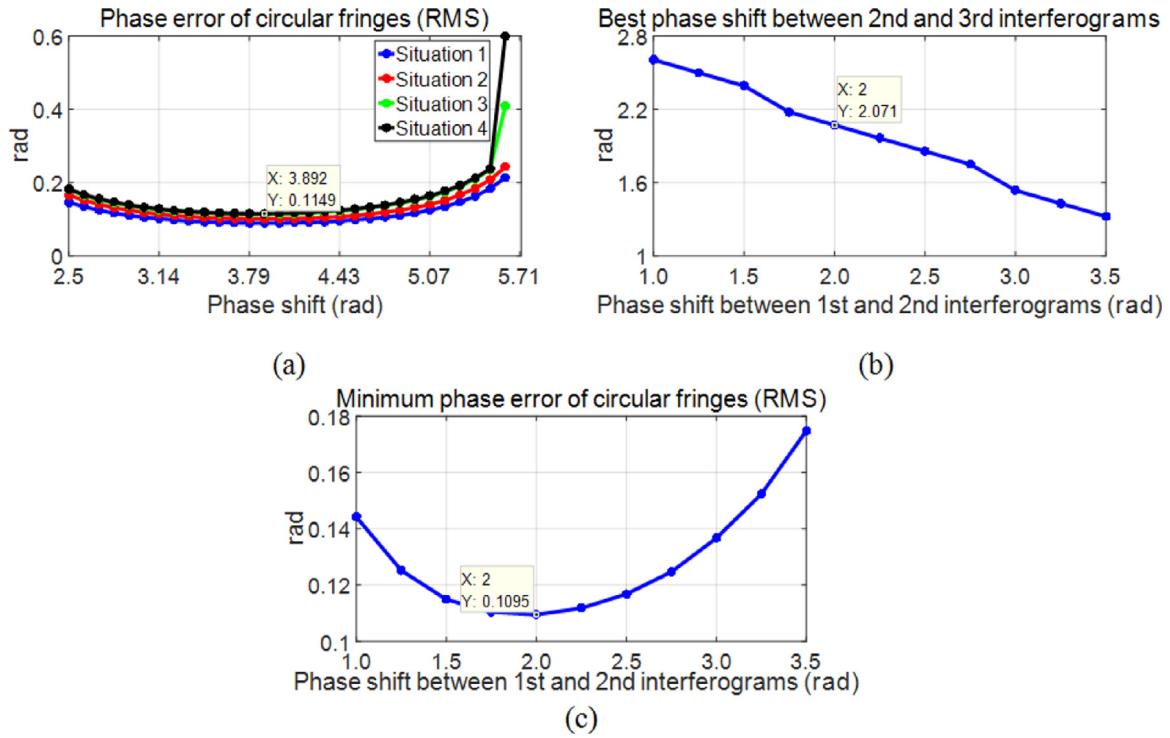


Fig. 9. The results of the circular fringes with different phase shifts using DN&FIA method. (a) RMS phase errors of different phase shifts when  $\theta_1 = 0, \theta_2 = 1.5$ , (b) the best phase shift between 2nd and 3rd interferograms with different phase shifts between 1st and 2nd interferograms, (c) the minimum RMS phase errors for the different phase shifts between 1st and 2nd interferograms in situation 4.

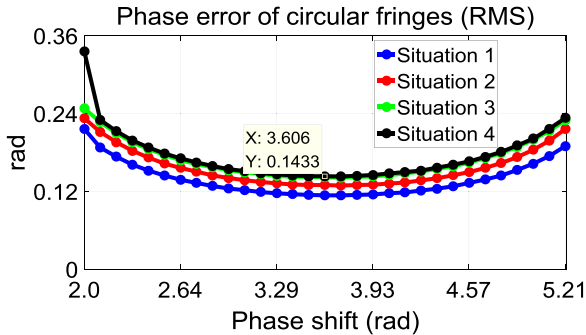


Fig. 10. The RMS phase errors of the circular fringes with different phase shifts using DN&FIA when the fringe number is 2.

number is 2, and other conditions are same as Fig. 8(a), the result is plotted in Fig. 10. From Fig. 10, we can see that, the best phase shift is same as the circular fringes when the fringe number is 5, so we can conclude that the fringe number will not affect the best relative phase shift.

Based on the above different simulations, the conclusions of the proposed DN&FIA can be summarized as: (1) It can achieve the high accuracy as AIA with less computational time by only three interferograms; (2) whether the circular, straight or complex fringes, the proposed method is valid; (3) the fringe numbers are best to be more than 2 if the high accuracy is requested; (4) the initial phase shifts of the iteration can be set randomly because different initial values will not affect the accuracy, and slightly affect the computational time; (5) the phase shift can be random except for the small practical phase shift  $(\theta_3 - \theta_2)/2$ , and the best relative phase shift between 2nd and 3rd interferograms is a variable value due to different relative phase shifts between 1st and

2nd interferograms, moreover, the fringe number will not affect the best relative phase shift.

#### 4. Demonstration with experimental data

In order to verify the performance of the proposed method, three groups of experiments are performed to do the phase retrieval by the proposed method and AIA. The experimental setup is Twyman–Green interferometer with 4D camera which is a kind of synchronous phase-shifting interferometer (SPSI) [30], four phase-shifted interferograms with the phase shifts  $0, \pi/2, \pi$  and  $3\pi/2$  can be extracted from a single image snapshot by the 12 bit polarization camera PolarCam with the pixel number of  $1208 \times 1348$  and the pixel size of  $7.4 \mu\text{m}$  from 4D Technology, Inc. [31–33], hence, the background intensity and modulation amplitude will be relatively stable between different phase shifted interferograms, that is to say, the experiment meets the condition of the assumption before Eq. (2). Moreover, we test different objects to capture the circular, straight and complex fringes, the objects are placed in the test arm. For the first experiment, three phase shifted interferograms with the circular fringes are collected, the size of the interferograms is  $401 \times 401$ , and the phase shifts are  $0, \pi/2$  and  $\pi$ . For DN&FIA, the initial phase shifts are respectively set as 0 rad and 1 rad, and only  $40 \times 40$  pixels are uniformly selected to take part in the iterative process. And, the initial phase shifts of AIA are respectively set as 0 rad, 1 rad and 3 rad. One of the interferograms is shown in Fig. 11(a), the extracted phase distributions using DN&FIA and AIA are shown in Fig. 11(b) and (c), Fig. 11(d) shows the difference between the phase distributions extracted by DN&FIA and AIA, the RMS value of the difference is only 0.0165 rad, we can get the same conclusion as the simulations, the accuracies of DN&FIA and AIA are similar. In addition, they both need 10 iterations, the iterative curves are plotted in Fig. 11(e) and (f), and the computational time of DN&FIA and AIA are respectively 1.8 s and 18.48 s, we can see that DN&FIA spends less time than AIA.

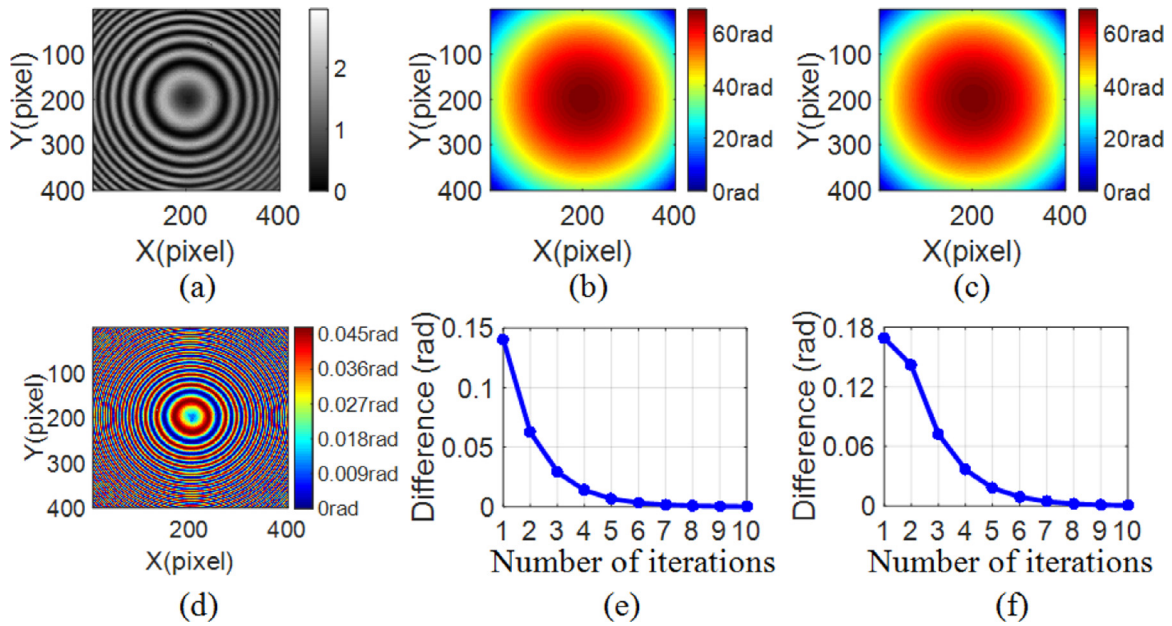


Fig. 11. Experimental results of the circular fringes. (a) One of the phase shifted interferograms, (b) and (c) the phase distributions extracted by DN&FIA (PV = 68.9120 rad, RMS = 14.2523 rad) and AIA (PV = 68.9074 rad, RMS = 14.2519 rad), (d) the difference between the phase distributions extracted by DN&FIA and AIA (RMS = 0.0165 rad), (e) and (f) the iterative curves of DN&FIA and AIA.

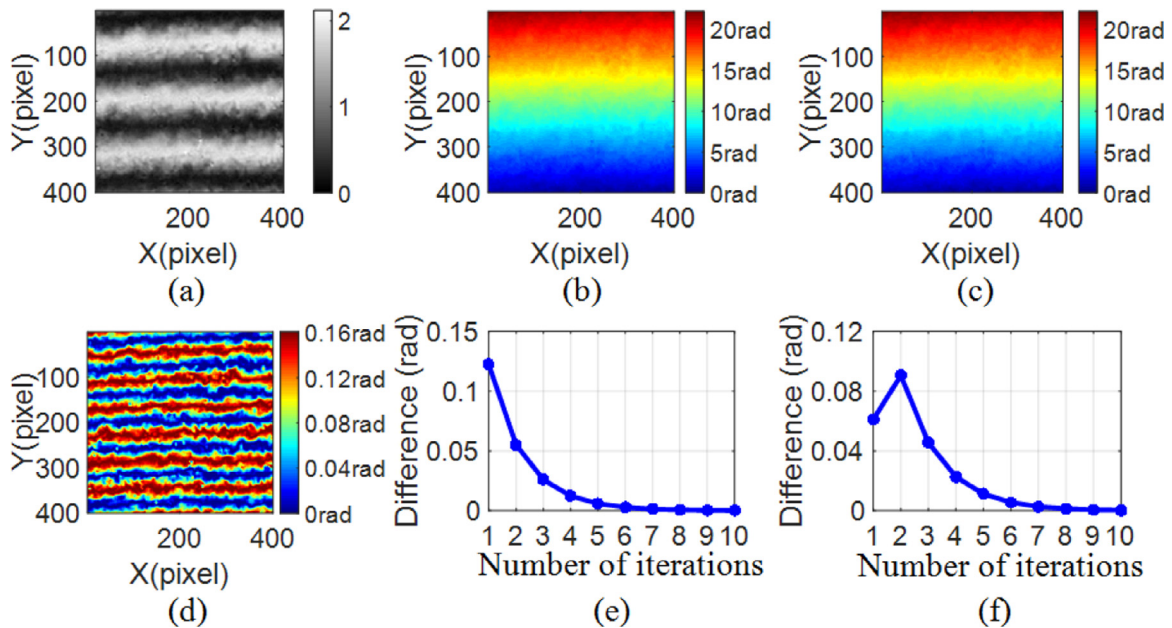


Fig. 12. Experimental results of the straight fringes. (a) One of the phase shifted interferograms, (b) and (c) the phase distributions extracted by DN&FIA (PV = 22.2001 rad, RMS = 6.0484 rad) and AIA (PV = 22.2026 rad, RMS = 6.0503 rad), (d) the difference between the phase distributions extracted by DN&FIA and AIA (RMS = 0.0564 rad), (e) and (f) the iterative curves of DN&FIA and AIA.

Then, the second and third experiments with the straight and complex fringes are performed, and the complex fringes are randomly obtained by the deformable mirror, the size of the interferograms with the straight fringes is also  $401 \times 401$ , and the size of the interferograms with the complex fringes is  $201 \times 201$ , other conditions are same as the above circular fringes. Figs. 12 and 13 show the results of the straight and complex fringes, we can see that, both DN&FIA and AIA are effective for the different fringes. Moreover, for the straight fringes, the RMS value of the difference between the phase distributions extracted by DN&FIA and AIA is 0.0564 rad, and the computational time for DN&FIA and AIA are

1.7 s and 18.30 s respectively. And, for the complex fringes, the RMS value of the difference between the phase distributions extracted by DN&FIA and AIA is 0.0507 rad, and the computational time for DN&FIA and AIA are 0.58 s and 4.15 s. For these two kinds of fringes, the accuracies are also similar for two methods, and for the computational time, we get the conclusion the same as the circular fringes. Through the above experiments, we verify that, for the circular, straight and complex fringes, the proposed DN&FIA can obtain relatively high measurement accuracy as AIA with less computational time by only three interferograms.

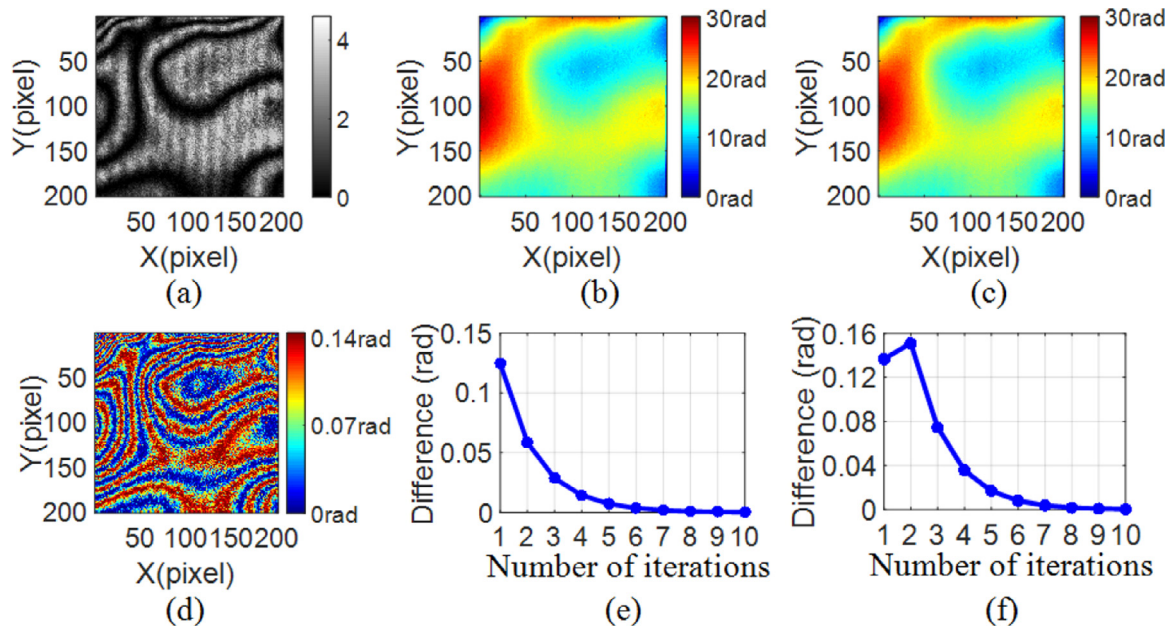


Fig. 13. Experimental results of the complex fringes. (a) One of the phase shifted interferograms, (b) and (c) the phase distributions extracted by DN&FIA (PV = 30.2191 rad, RMS = 4.3279 rad) and AIA (PV = 30.0985 rad, RMS = 4.3262 rad), (d) the difference between the phase distributions extracted by DN&FIA and AIA (RMS = 0.0507 rad), (e) and (f) the iterative curves of DN&FIA and AIA.

## 5. Conclusion

In this paper, we present a PSA based on difference map normalization and fast iterative algorithm, the difference maps are obtained by three phase shifted interferograms firstly, and then normalization is performed for the difference maps, the results are just as two phase shifted interference signals without the background intensity. Next the least-squares algorithm is applied to extract the phase distribution, and only a limited number of samples are chosen to take part in the iterative process to save time. We have compared DN&FIA with AIA by the simulated data and experimental data. The proposed algorithm can achieve high measurement accuracy as AIA, and cost less time than AIA, and the fringe numbers are best to be more than 2 if the high accuracy is requested. In addition, the initial phase shifts of the iteration can be random, and the phase shifts can be random except for the small practical phase shift  $(\theta_3 - \theta_2)/2$ . Finally, the proposed algorithm is effective for the circular, straight or complex fringes. The simulations and experiments demonstrate the validity of the proposed method. In summary, this proposed method is a power tool for the phase retrieval with random phase shift.

## Funding

This work was supported by the National Natural Science Foundation of China (NSFC) (11304034); Program of China Scholarship Council (201508220104); Program of Jilin Provincial Educational Department (JJKH20190691KJ); State Key Laboratory of Applied Optics; Doctoral Research Foundation of Northeast Electric Power University (BSJXM-201218); and Scientific Basic Research Foundation of Northeast Electric Power University.

## Supplementary materials

Supplementary material associated with this article can be found, in the online version, at [doi:10.1016/j.optlaseng.2019.03.010](https://doi.org/10.1016/j.optlaseng.2019.03.010).

## References

[1] Malacara D. *Optical shop testing*. 3rd ed. John Wiley & Sons, Inc; 2007. Chap 1-7.

- [2] Bruning JH, Herriott DR, Gallagher JE, Rosenfeld DP, White AD, Brangaccio DJ. Digital wavefront measuring interferometer for testing optical surfaces and lenses. *Appl Opt* 1974;13(11):2693–703. <https://doi.org/10.1364/AO.13.002693>.
- [3] Tian C, Liu S. Two-frame phase-shifting interferometry for testing optical surfaces. *Opt Express* 2016;24(16):18695–708. <https://doi.org/10.1364/OE.24.018695>.
- [4] Malacara D. *Optical shop testing*. 3rd ed. John Wiley & Sons, Inc; 2007. Chap 14.
- [5] de Groot PJ. Vibration in phase-shifting interferometry. *J Opt Soc Am A* 1995;12(2):354–65. <https://doi.org/10.1364/JOSAA.12.000354>.
- [6] Deck LL. Suppressing phase errors from vibration in phase-shifting interferometry. *Appl Opt* 2009;48(20):3948–60. <https://doi.org/10.1364/AO.48.003948>.
- [7] Wang Z. Advanced iterative algorithm for phase extraction of randomly phase-shifted interferograms. *Opt Lett* 2004;29(14):1671–3. <https://doi.org/10.1364/OL.29.001671>.
- [8] Xu J, Xu Q, Chai L. Iterative algorithm for phase extraction from interferograms with random and spatially nonuniform phase shifts. *Appl Opt* 2008;47(3):480–5. <https://doi.org/10.1364/AO.47.000480>.
- [9] Chen Y-C, Lin P-C, Lee C-M, Liang C-W. Iterative phase-shifting algorithm immune to random phase shifts and tilts. *Appl Opt* 2013;52(14):3381–6. <https://doi.org/10.1364/AO.52.003381>.
- [10] Farrell CT, Player MA. Phase step measurement and variable step algorithms in phase-shifting interferometry. *Meas Sci Technol* 1992;3:953–8. <http://doi.org/10.1088/0957-0233/3/10/003>.
- [11] Liu F, Wang J, Wu Y, Wu F, Trusiak M, Patorski K, Wan Y, Chen Q, Hou X. Simultaneous extraction of phase and phase shift from two interferograms using Lissajous figure and ellipse fitting technology with Hilbert-Huang prefiltering. *J Optics-UK* 2016;18:105604. <http://doi.org/10.1088/2040-8978/18/10/105604>.
- [12] Cai LZ, Liu Q, Yang XL, Wang YR. Sensitivity adjustable contouring by digital holography and a virtual reference wavefront. *Opt Commun* 2003;221:49–54. [https://doi.org/10.1016/S0030-4018\(03\)01468-8](https://doi.org/10.1016/S0030-4018(03)01468-8).
- [13] Cai LZ, Liu Q, Yang X L. Phase-shift extraction and wave-front reconstruction in phase-shifting interferometry with arbitrary phase steps. *Opt Lett* 2003;28(19):1808–10. <https://doi.org/10.1364/OL.28.001808>.
- [14] Cai LZ, Liu Q, Yang XL. Generalized phase-shifting interferometry with arbitrary unknown phase steps for diffraction objects. *Opt Lett* 2004;29(2):183–5. <https://doi.org/10.1364/OL.29.000183>.
- [15] Meng XF, Cai LZ, Xu XF, Yang XL, Shen XX, Dong GY, Wang YR. Two-step phase-shifting interferometry and its application in image encryption. *Opt Lett* 2006;31(10):1414–16. <https://doi.org/10.1364/OL.31.001414>.
- [16] Xu XF, Cai LZ, Meng XF, Dong GY, Shen XX. Fast blind extraction of arbitrary unknown phase shifts by an iterative tangent approach in generalized phase-shifting interferometry. *Opt Lett* 2006;31(13):1966–8. <https://doi.org/10.1364/OL.31.001966>.
- [17] Xu XF, Cai LZ, Wang YR, Yang XL, Meng XF, Dong GY, Shen XX, Zhang H. Generalized phase-shifting interferometry with arbitrary unknown phase shifts: direct wave-front reconstruction by blind phase shift extraction and its experimental verification. *Appl Phys Lett* 2007;90:121124. <https://doi.org/10.1063/1.2716069>.
- [18] Xu XF, Cai LZ, Wang YR, Meng XF, Sun WJ, Zhang H, Cheng XC, Dong GY, Shen XX. Simple direct extraction of unknown phase shift and wavefront reconstruction in generalized phase-shifting interferometry: algorithm and experiments. *Opt Lett* 2008;33(8):776–8. <https://doi.org/10.1364/OL.33.000776>.

- [19] Xu XF, Cai LZ, Wang YR, Yan RS. Direct phase shift extraction and wave-front reconstruction in two-step generalized phase-shifting interferometry. *J Opt* 2010;12(1):015301. <https://doi.org/10.1088/2040-8978/12/1/015301>.
- [20] Yan RS, Cai LZ, Meng XF. Correction of wave-front retrieval errors caused by the imperfect collimation of reference beam in phase-shifting interferometry. *Optik* 2014;125(2):601–5. <https://doi.org/10.1016/j.ijleo.2012.05.054>.
- [21] Vargas J, Quiroga J, Belenguer T. Phase-shifting interferometry based on principal component analysis. *Opt Lett* 2011;36(8):1326–8. <https://doi.org/10.1364/OL.36.001326>.
- [22] Vargas J, Quiroga J, Belenguer T. Analysis of the principle component algorithm in phase-shifting interferometry. *Opt Lett* 2011;36(12):2215–17. <https://doi.org/10.1364/OL.36.002215>.
- [23] Deng J, Wang K, Wu D, Lv X, Li C, Hao J, Qin J, Chen W. Advanced principal component analysis method for phase reconstruction. *Opt Express* 2015;23(9):12222–31. <https://doi.org/10.1364/OE.23.012222>.
- [24] Xu J, Jin W, Chai L, Xu Q. Phase extraction from randomly phase-shifted interferograms by combining principal component analysis and least squares method. *Opt Express* 2011;19(21):20483–92. <https://doi.org/10.1364/OE.19.020483>.
- [25] Yatabe K, Ishikawa K, Oikawa Y. Improving principal component analysis based phase extraction method for phase-shifting interferometry by integrating spatial information. *Opt Express* 2016;24(20):22881–91. <https://doi.org/10.1364/OE.24.022881>.
- [26] Yatabe K, Ishikawa K, Oikawa Y. Simple, flexible and accurate phase retrieval method for generalized phase-shifting interferometry. *J Opt Soc Am A* 2017;34(1):87–96. <https://doi.org/10.1364/JOSAA.34.000087>.
- [27] Yatabe K, Ishikawa K, Oikawa Y. Hyper ellipse fitting in subspace method for phase-shifting interferometry: practical implementation with automatic pixel selection. *Opt Express* 2017;25(23):29401–16. <https://doi.org/10.1364/OE.25.029401>.
- [28] Vargas J, Quiroga J, Sorzano C, Estrada J, Carazo J. Two-step demodulation based on the Gram-Schmidt orthonormalization method. *Opt Lett* 2012;37(3):443–5. <https://doi.org/10.1364/OL.37.000443>.
- [29] Wang H, Luo C, Zhong L, Ma S, Lu X. Phase retrieval approach based on the normalized difference maps induced by three interferograms with unknown phase shifts. *Opt Express* 2014;22(5):5147–54. <https://doi.org/10.1364/OE.22.005147>.
- [30] Zhang Y, Tian X, Liang R. Fringe-print-through error analysis and correction in snapshot phase-shifting interference microscope. *Opt Express* 2016;25(22):26554–66. <https://doi.org/10.1364/OE.25.026554>.
- [31] Novak M, Miller J, Brock N, North-Morris M, Hayes J, Wyant J. Analysis of a micropolarizer array-based simultaneous phase-shifting interferometer. *Appl Opt* 2015;44(32):6861–8. <https://doi.org/10.1364/AO.44.006861>.
- [32] Wang D, Liang R. Simultaneous polarization Mirau interferometer based on pixelated polarization camera. *Opt Lett* 2016;41(1):41–4. <https://doi.org/10.1364/OL.41.000041>.
- [33] <https://www.4dtechnology.com/products/polarimeters/polarcam/>.